Journal of Nuclear Materials 467 (2015) 677–682

Contents lists available at ScienceDirect

Journal of Nuclear Materials

journal homepage: www.elsevier.com/locate/jnucmat

Mechanical properties of irradiated nanowires – A molecular dynamics study

Emilio Figueroa [a, b], Diego Tramontina [c, d], Gonzalo Gutiérrez [a, *], Eduardo Bringa [c]

[a] Grupo de NanoMateriales, Departamento de Física, Facultad de Ciencias, Universidad de Chile, Casilla, 653 Santiago, Chile
[b] Departamento de Física, Facultad de Ciencias Naturales, Matemática y del Medio Ambiente, Universidad Tecnológica Metropolitana, Santiago 7800002, Chile
[c] Facultad de Ciencias Exactas y Naturales, Universidad Nacional de Cuyo, 5500 Mendoza, Argentina
[d] Instituto de Bioingeniería, Universidad de Mendoza, 5500 Mendoza, Argentina

HIGHLIGHTS

- Stacking Fault Tetrahedra (SFT) formation proceeds by cascades, containing typically a vacancy cluster and interstitials.
- Applied tension leads to the destruction of the SFT, in contrast to a recently reported case of a SFT which soften the NW.
- After the initial dislocation activity, strength is controlled by a few surviving dislocations.

ARTICLE INFO

Article history:
Received 10 August 2015
Received in revised form
19 October 2015
Accepted 22 October 2015
Available online 26 October 2015

Keywords:
Radiation damage
Nanowires
Mechanical properties
Computer simulation

ABSTRACT

In this work we study, by means of molecular dynamics simulation, the change in the mechanical properties of a gold nanowire with pre-existing radiation damage. The gold nanowire is used as a simple model for a nanofoam, made of connected nanowires. Radiation damage by keV ions leads to the formation of a stacking fault tetrahedron (SFT), and this defect leads to a reduced plastic threshold, as expected, when the nanowire is subjected to tension. We quantify dislocation and twin density during the deformation, and find that the early activation of the SFT as a dislocation source leads to reduced dislocation densities compared to the case without radiation damage. In addition, we observed a total destruction of the SFT, as opposed to a recent simulation study where it was postulated that SFTs might act as self-generating dislocation sources. The flow stress at large deformation is also found to be slightly larger for the irradiated case, in agreement with recent experiments.

1. Introduction

Studies of materials under irradiation are needed in fields that go from medicine to astrophysics. Radiation damage includes the formation of point, line and volumetric defects: clusters of vacancies or interstitials, dislocation loops, stacking faults, twins, and stacking fault tetrahedra (SFTs) [1–3]. A single high energy recoil can form SFTs according to simulations [4,5], but they can also be formed by quenching [6], or high strain-rate deformation [7], since they can evolve from a vacancy cluster in many fcc metals [8]. SFTs significantly change the mechanical properties of a material, offering a strong obstacle to dislocation motion [9,5], and there are several recent efforts to reduce their density after irradiation [10–12]. For instance, current research has shown how a SFT is fully absorbed by screw dislocation [13,14].

The irradiation of nanostructures display distinct characteristics, compared to bulk samples [4]. Recently, it was shown that nanofoams can be radiation-resistant, due to their large surface-to-volume ratio which leads to surface defect sinks [15]. However, it was also shown that more energetic irradiation at higher dose leads to the formation of SFTs in Au nanofoams, despite the nanometer scale of the foam filaments [16]. Something similar happens in Ag nanofoams [17]. Experimental Au foams in those studies had interconnected nanowires with a diameter around 30 nm and a

* Corresponding author.
E-mail address: gonzalo@fisica.ciencias.uchile.cl (G. Gutiérrez).

http://dx.doi.org/10.1016/j.jnucmat.2015.10.036
0022-3115/

length around 60 nm. Simulations of nanofoams at those scales would require tremendous computational power, and atomistic simulations are typically carried out with foams with filament diameters one order of magnitude below those experimental values [18]. In order to understand possible effects from the much larger wire diameter, simulations have also been carried out for single nanowires under irradiation [15,16]. Aiming to study the effect of radiation damage in the mechanical properties of foams, recently Zepeda-Ruiz et al. [10] created a perfect SFT, with a side of 5.5 nm, and carved a cylindrical nanowire around it, with 10 nm diameter and 20 nm length. This nanowire was compressed along its axis, resulting in the SFT acting as a dislocation source and reducing the elastic limit, because the surface sources activate at much higher stress. Detailed analysis of dislocation reactions was carried out, showing that the SFT was nearly re-generated, therefore making possible a Frank-Read-like dislocation source. However, a recent simulation [19] of a cross-array of two nanowires with a 10 nm diameter had a lower plastic threshold than a single nanowire, even with an SFT as source, because the junction itself facilitates dislocation nucleation. On the other hand, nanoindentation experiments [19] showed irradiation lead to nanofoam hardening, and this was explained as regular hardening due to dislocation–obstacle interaction.

Irradiation of nanostructures has been shown to affect mechanical properties [20–22]. Other properties such as the sputtering yield may also be affected [23]. Irradiation of nanowires in particular has been shown to be strongly size-dependent. For instance, Kiener et al. [24] studied Cu nanopillars with 80–1500 nm diameter. Below 400 nm diameter, there was size-dependent strength under compression from a nanoindenter, explained by dislocation source limitation. Pillars were irradiated by 1.1 MeV H irradiation up to 0.8 *dpa*, generating dislocations and other defects, including 0.5–3 nm SFTs, which then lead to strength controlled by the activation stress of the sources introduced by irradiation.

Regarding simulations, there is a long tradition of atomistic simulations of the mechanical properties of NWs but most simulations have been carried out for perfect single-crystal samples [25]. Amongst the few exceptions it can be mentioned the work by Farkas on polycrystalline NW, and the recent work by Srolovitz and co-workers on polycrystalline and nanotwinned NWs [26]. Espinosa and co-workers [27] simulated NWs with dislocation sources using dislocation dynamics, but atomistic simulation of NWs with pre-existing dislocation sources other than GBs is lacking. Yu et al. [28] recently studied the coupling effects of stress and ion irradiation on the mechanical behaviors of copper nanowires, with $D = 12$ nm and 1–10 keV PKA from the surface of the NW. They found that the elastic limit decreases with PKA energy, and after 7% strain, there are only few defect clusters left inside the NW, with no partials and no twins evident in the snapshots they provided. The work by Zepeda-Ruiz et al. [10] is also an important step to understand Au Nws with radiation damage.

Here we present a molecular dynamics simulation study about the effects of a pre-existing radiation damage on the mechanical properties of gold nanowire, and offer an alternative, significantly different scenario for the mechanical response of a radiation-damaged NW. For this purpose, we first generate, by means of a 20 keV collision cascade, a large defective region in the sample, which after 0.1 ns since the beginning of the bombardment transform into a SFT and other point defects. Then, we perform a tensile test for both the pristine and irradiated gold nanowire, providing an atomic level description, such as the dislocation and twin density during the deformation. The paper is organized as follows: in Section 2 we explain the methodology. The results are presented in Section 3, and finally, in Section 4 we draw some concluding remarks.

2. Computational methodology

The molecular dynamics simulations on Au NW were performed using LAMMPS [29], with an embedded atom method (EAM) potential [30] modified with the Ziegler, Biersack and Littmark (ZBL) [31] for radiation damage simulations. With the aim of mimicking the radiation conditions in the recent paper by Fu et al. [16], a primary knock-on atom (PKA) of 20 keV is simulated at the center of a Au nanowire with a diameter of 25 nm and length of about 50 nm, close to experimental sizes, comprising 1.5 millions atoms. The z axis runs along the [001] direction, where periodic boundary conditions were applied. Several different PKAs were run in the pristine cylinder, and although this high energy cascade leads to melting of a relatively large volume, the top/bottom boundaries were unaffected. Also, we found many events which produced a SFT from a single recoil. The defects that resulted from the irradiation were analyzed during the cascade and after the nanowires returned to nearly 300 K, using OVITO [32], with adaptive common neighbor analysis [33], and bond-angle analysis (BAA) [34] to identify defects, as well as the diagnostic tools provided by LPMD package [35].

The final defective configuration was relaxed for ~0.2 ns, and we take the wire down to 10 K. Only a few point defects remain alongside the SFT, which has a final side length of about ~4 nm. This size is within the typical size-range of radiation induced SFTs [36]. Then, we apply uniaxial tension to both perfect and defective wires, at strain rates of 10^8 s^{-1}.

3. Results

In the following we first describe the results of the radiation damage, and then the tensile test in the unirradiated and the irradiated Au NW.

3.1. Irradiation-induced stacking fault tetrahedra formation

Cascade evolution in bulk materials has been extensively studied [37]. However, much less is known of cascades in nanostructures [38]. In our simulations, the NW size is well within the nanoscale, but large enough to easily contain a typical collision cascade of 20 keV. Fig. 1 shows snapshots of the cascade evolution. Fig. 1(a) displays the maximum extent of the cascade, with a molten core and a few straight collision sequences leaving a trail of defects behind. In Fig. 1(b) can be seen how few stacking faults bound by partial dislocations are generated around the central zone, due to the large stress in the cascade [39]. SFs can grow and reach the NW surface, and are a typical deformation mode for NWs under stress [25]. As the cascade cools down in Fig. 1(c), the SF are re-absorbed, and in Fig. 1(d) only one SFT and some point defect remains.

At the end of our simulations (~0.2 ns after the PKA started), an SFT was often formed, together with a number of point defects, and vacancy and interstitial loops. One such case is shown in Fig. 2. We compare: (a) adaptive CNA [33], and (b) bond-angle analysis [34]. Both analysis show that one corner of this tetrahedron is incomplete, similar to what was observed in Cu [4].

Fig. 3 shows atoms with displacement greater than $a_0/2$ with respect to their original position, viewed along $[1\bar{1}0]$. The SFT can be observed as a triangular shape in the center of the cluster of displaced atoms. There are two clear replacement collision sequences observed, center-left, and top-right of the figure. The final number of displaced atoms can be used to estimate *dpa* (displacements per atom) for this single irradiation, giving $dpa \approx 0.005$, as expected an extremely small irradiation dose compared to typical conditions in a nuclear reactor. Wigner-Seitz analysis carried out with OVITO [32] results in 220 Frenkel pairs of individual vacancies and interstitials at the end of the cascade.

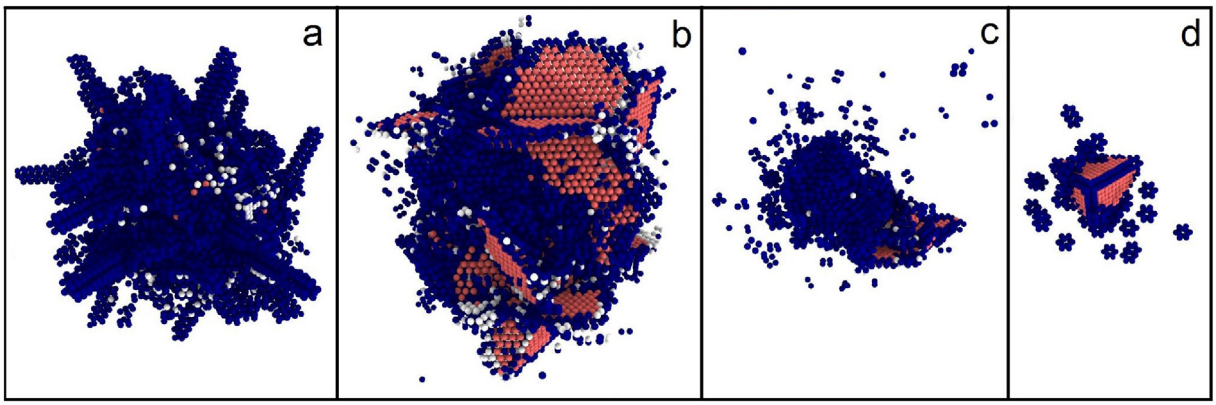

Fig. 1. Snapshots of the cascade evolution, for different times after the PKA started. Local crystalline structure is shown by the different colors (red: hcp atoms, white: bcc, blue: no structure, including atoms in partial dislocations), and all fcc atoms were deleted. (a) 0.5 ps; (b) 5 ps; (c) 30 ps; (d) 215 ps. (For interpretation of the references to colour in this figure legend, the reader is referred to the web version of this article.)

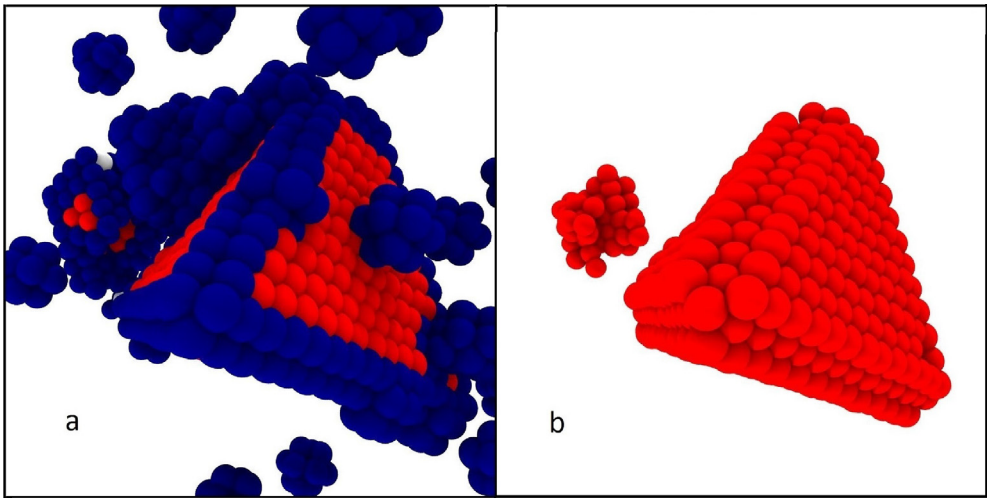

Fig. 2. Stacking fault tetrahedron (SFT), created by a single collision cascade, ~0.2 ns after the PKA started. (a) shows CNA analysis as in Fig. 1. (b) bond-angle analysis [34] filtering, to show only hcp atoms.

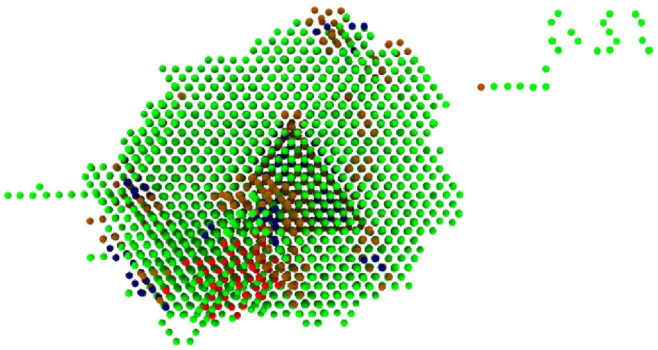

Fig. 3. Atoms in the final configuration, which are displaced more than $a_0/\sqrt{2}$ with respect to their original position, viewed along $[1\bar{1}0]$. Local crystalline structure is shown by the different colors (green: fcc; red: twin boundaries; blue: stacking faults, brown: unidentified atoms.). (For interpretation of the references to colour in this figure legend, the reader is referred to the web version of this article.)

3.2. Tensile test

Fig. 4 shows the activation of surface sources in the perfect NW, as observed before [25]. Multiple sources are activated nearly simultaneously, resulting in closely spaced SFs in {111} planes, and the subsequent formation of nano-twins. Surface steps resulting from SFs reaching the surface can be observed. There is profuse intersection of SFs. At ~10% the hardening of the NW can be associated to a dislocation outburst. The activation of surface sources leads to a large stress release. The outline of the NW in Fig. 1(d) can be seen to be fairly cylindrical, without the typical shear localization observed in experiments [40].

The deformation of the irradiated NW is significatively different. Fig. 5 displays a sequence of snapshots corresponding to the emission of dislocations and twins at different strains. At the beginning, the SFT is surrounded by point defects. Then, the SFT disappears during elongation of the NW, with multiple SFs shearing the SFT, in a process similar to the one used to explain defect-free channels in radiation damage of Cu [9]. The final configuration of the NW includes {111} surface terraces due to slip traces, and looks similar to experimental configurations of nanowires under tension [40], unlike the case of the unirradiated NW.

We quantify the structure defects by use of the Crystal Analysis Tool [33], as shown in Fig. 6, for atoms in intrinsic SFs and in twins. Extrinsic SFs can be neglected with respect to intrinsic SFs in the simulated cases. Partial dislocations bound SFs which propagate across the NW. In the perfect NW, a large SF density is produced by

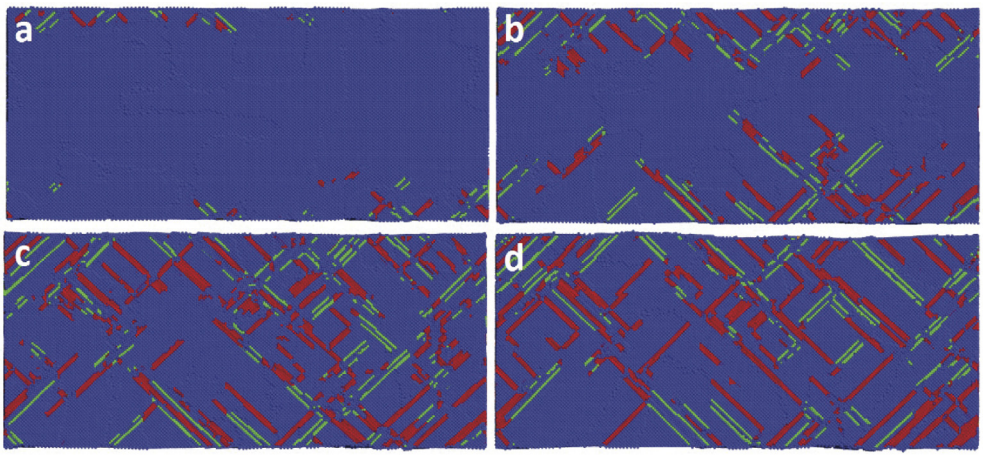

Fig. 4. Cross-section of the unirradiated sample under 10^8 s^{-1} uniaxial deformation at ε=10.09,10.15,10.18 and 10.35%. Red, green and blue indicate stacking faults, twin boundaries and regular f.c.c. atoms respectively. In (a) dislocations are nucleated at the surface; in (b) they propagate across the NW; in (c) and (d) the whole NW is cross-crossed by planar defects. (For interpretation of the references to colour in this figure legend, the reader is referred to the web version of this article.)

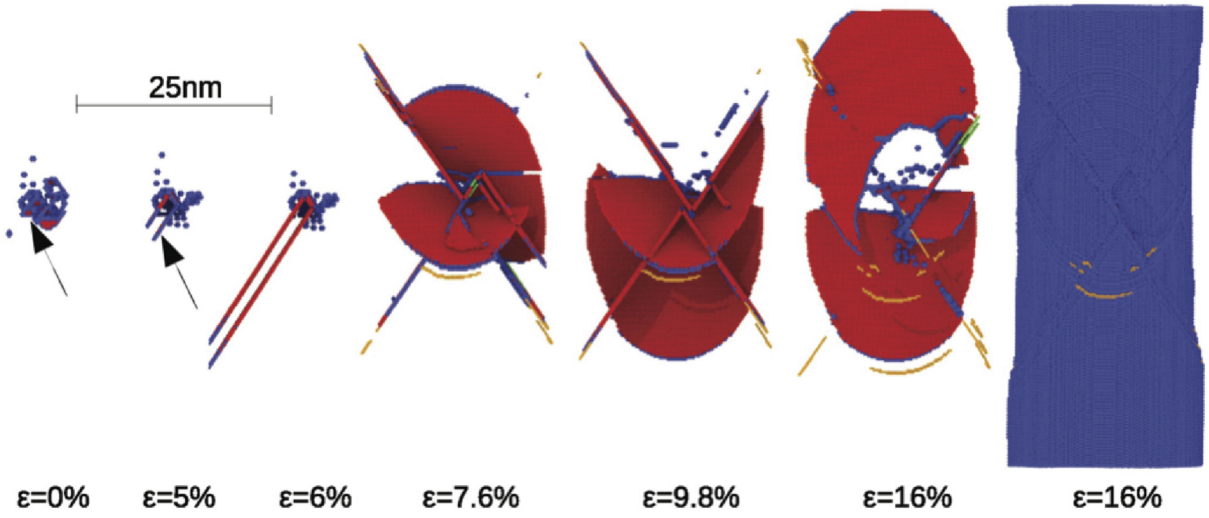

Fig. 5. Nanowire with pre-existing radiation damage. The figure shows the initial SFT surrounded by point defects at ε=0 and shows the emission of partial dislocations and twins from the SFT for ε=5,6,7.6,9.8,16%, removing all f.c.c. atoms. The last snapshot shows the whole sample for ε=16%. Red, green and blue indicate stacking faults, twin boundaries and another atoms respectively. (For interpretation of the references to colour in this figure legend, the reader is referred to the web version of this article.)

surface sources, accompanied by twin formation. According to Orowan's equation, plastic relaxation is proportional to the product of dislocation density and dislocation velocity. For the case of pre-existing sources, dislocations are nucleated at a lower stress, and they can move more freely to relax the material. For the case of a perfect NW, multiple surface sources lead to numerous dislocation junctions which typically hinder dislocation motion. A similar situation has been explored for high strain rate loading of bulk fcc metals [41]. We note that there is a large nanotwin density, which can vary significantly. NW with pre-existing nanotwins can be made experimentally, and have been shown to display interesting mechanical properties [12]. Stress-strain curves can also be seen in Fig. 6, and the elastic limit for the perfect nanowire is reached at a strain of about 10%. The sudden activation of multiple surface sources leads to a catastrophic stress decrease, down to a flow stress of about 1 GPa at large strain, together with the associated immense increase in stacking faults and twins. Similar results have been reported, but rarely including detailed dislocation analysis. The curve for the defective NW shows a significantly reduced elastic limit, of about 2 GPa and ~3% of strain. Dislocation emission from the SFT leads to this lower plastic yield, as in Ref. [10]. However, the SFT capability as a dislocation source is limited and it does not behave as a Frank-Read type source, unlike what was observed under compression for a smaller NW [10]. This early emission leads to relaxation of the sample without requiring the huge dislocation density observed in the perfect NW: dislocations can move further because less junctions are formed. This reduction in dislocation density also leads to a significant reduction in twin formation. SF density is 4 times lower, but the flow stress between 12 and 16% strain is higher than the flow stress in the perfect NW, which does not have any point defects or defect clusters. We have carried out simulations for other NW with a radiation-induced SFT and we observe similar qualitative behavior, and the final flow stress can be even 20–30% larger than for the perfect NW. This hardening can also be observed in the NW under compression, as it can be seen in the inset of Fig. 6. We note that in this case the SFT does not disappear [10] as in the tension case.

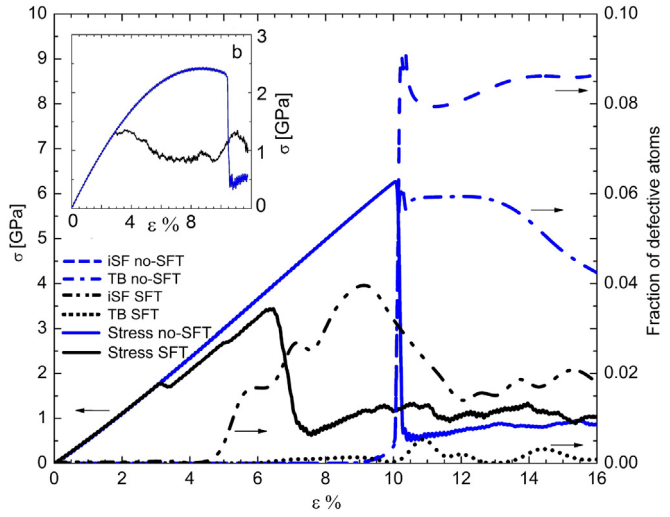

Fig. 6. Stress-strain curves (solid lines, left vertical axis) and defects (dashed lines, right vertical axis) for unirradiated NW (blue) and irradiated NW (black) (iSF: intrinsic stacking faults; TB: twin boundaries). Inset shows stress–strain curves for the same NW under compression, also displaying hardening at large strains. (For interpretation of the references to colour in this figure legend, the reader is referred to the web version of this article.)

4. Concluding remarks

Regarding the SFT formation, the results of our simulations indicate that a SFT can form directly within a 25 nm Au nanowire, due to a 20 keV recoil. This is similar to what has been shown for bulk cascades [4,5], and there is no need for multiple cascades and vacancy diffusion, as in lower energy cascades of few keVs [16]. The formation proceeds nearly in the same way described for bulk cascades. In this case we carry out detailed structural analysis during the cascade evolution and show, after the ballistic phase of the cascade, the formation of SFs bounded by partial dislocations, which sometimes reach the surface of the NW. However, this SFs mostly recover, but contribute to the final SFT which appears clearly as the cascade-induced thermal spike cools down. This final SFT contains typically a vacancy cluster, but also a number of interstitials. This differs from some scenarios where SFTs are formed by vacancy migration and clustering and assumed completely hollow [10], and also from other scenarios where SFTs can be deprived of vacancies at their core [42].

Summarizing our results of the tensile test, we find that a nanowire (NW) with a Stacking Fault Tetrahedra (SFT) and point defects resulting from radiation damage has a lower elastic limit than a perfect NW, as expected. Applied tension of such defective nanowire leads to the destruction of the SFT. This is different from the recently reported case of a SFT which soften the NW but regenerates under compression [10]. The SFT in this study is smaller, it is contained in a much larger nanowire, and we focus on deformation under tension, and up to larger strains. The final configuration of our simulated NW resembles experimental results [40], with slip traces deforming significantly the outer surface of the NW. After the initial dislocation activity, strength is controlled by a few surviving dislocations, while the initial radiation defects have been mostly eliminated.

For nanofoams, it has been proposed that NW junctions play a crucial role in lowering of the plastic yield, irrespective of radiation damage [19]. Experiments in the same study showed that 1 *dpa* dose lead to a hardening increase of 15%. Here we have a dose below 0.5 *dpa* and find a 10% hardening increase, due to the interaction of dislocations with defects, despite the fact that the original SFT was mostly destroyed under tension. A similar hardening effect is found under compression.

A direct connection between the properties of NWs and realistic nanofoams which include grain boundaries, growth twins and other defects is challenging, but our results show the complex scenario which might arise for defective NWs, and point to the need for more simulations and experiments which might clarify the role of defects in the mechanical properties of nanostructures.

Acknowledgments

We acknowledge support from Bilateral project CONICYT ACE-01 Chile, ANPCyT-PICT2697 Argentina, and CONICYT-PIA grant ACT-1115, Chile. EMB and DT thank support from PICT-PRH-0092 and a SeCTyP grant. We also thank discussions with E. Martinez, A. Caro and M. Caro.

References

[1] Y. Shimomura, R. Nishiguchi, Radiat. Eff. Defects Solids 141 (1997) 311–324.
[2] M. Kiritani, Mater. Chem. Phys. 50 (1997) 133–138.
[3] K. Yu, D. Bufford, F. Khatkhatay, H. Wang, M. Kirk, X. Zhang, Scr. Mater. 69 (2013) 385–388.
[4] K. Nordlund, F. Gao, Appl. Phys. Lett. 74 (1999) 2720–2722.
[5] Y.N. Osetsky, R. Stoller, D. Rodney, D. Bacon, Mater. Sci. Eng. A 400401 (2005) 370–373. Dislocations 2004. An International Conference on the Fundamentals of Plastic Deformation.
[6] J. Silcox, P.B. Hirsch, Philos. Mag. 4 (1959) 72–89.
[7] M. Kiritani, Y. Satoh, Y. Kizuka, K. Arakawa, Y. Ogasawara, S. Arai, Y. Shimomura, Philos. Mag. Lett. 79 (1999) 797–804.
[8] B.P. Uberuaga, R.G. Hoagland, A.F. Voter, S.M. Valone, Phys. Rev. Lett. 99 (2007) 135501.
[9] B. Wirth, V. Bulatov, T.D. de la Rubia, J. Nucl. Mater. 283–287 (Part 2) (2000) 773–777, 9th Int. Conf. on Fusion Reactor Materials.
[10] L.A. Zepeda-Ruiz, E. Martinez, M. Caro, E.G. Fu, A. Caro, Appl. Phys. Lett. 103 (2013) 031909.
[11] X. Zhang, E.G. Fu, L. Shao, H. Wang, N. Li, A. Misra, J.Y.-Q. Wang, J. Eng. Mater. Technol. 134 (2013) 041010.
[12] K.Y. Yu, D. Bufford, C. Sun, Y. Liu, H. Wang, M.A. Kirk, M. Li, X. Zhang, Nat. Commun. 4 (2013) 1377.
[13] H. Fan, J.A. El-Awady, Q. Wang, J. Nucl. Mater. 458 (2015a) 176–186.
[14] H. Fan, Q. Wang, C. Ouyang, J. Nucl. Mater. 465 (2015b) 245–253.
[15] E.M. Bringa, J.D. Monk, A. Caro, A. Misra, L. Zepeda-Ruiz, M. Duchaineau, F. Abraham, M. Nastasi, S.T. Picraux, Y.Q. Wang, D. Farkas, Nano Lett. 12 (2012) 3351–3355.
[16] E.G. Fu, M. Caro, L.A. Zepeda-Ruiz, Y.Q. Wang, K. Baldwin, E. Bringa, M. Nastasi, A. Caro, Appl. Phys. Lett. 101 (2012) 191607.
[17] C. Sun, D. Bufford, Y. Chen, M.A. Kirk, Y.Q. Wang, M. Li, H. Wang, S.A. Maloy, X. Zhang, Sci. Rep. 4 (2014).
[18] D. Farkas, A. Caro, E. Bringa, D. Crowson, Acta Mater. 61 (2013) 3249–3256.
[19] M. Caro, W.M. Mook, E.G. Fu, Y.Q. Wang, C. Sheehan, E. Martinez, J.K. Baldwin, A. Caro, Appl. Phys. Lett. 104 (2014).
[20] D. Jang, X. Li, H. Gao, J.R. Greer, Nat. Nanotechnol. 7 (2012) 594–601.
[21] Y. Kulkarni, R.J. Asaro, Acta Mater. 57 (2009) 4835–4844.
[22] Z. Wu, Y. Zhang, D. Srolovitz, Acta Mater. 57 (2009) 4508–4518.
[23] G. Greaves, J.A. Hinks, P. Busby, N.J. Mellors, A. Ilinov, A. Kuronen, K. Nordlund, S.E. Donnelly, Phys. Rev. Lett. 111 (2013) 065504.
[24] D. Kiener, P. Hosemann, S.A. Maloy, A.M. Minor, Nat. Mater. 10 (2011) 608–613.
[25] C.R. Weinberger, W. Cai, J. Mater. Chem. 22 (2012) 3277–3292.
[26] Z. Wu, Y. Zhang, M. Jhon, J. Greer, D. Srolovitz, Acta Mater. 61 (2013) 1831–1842.
[27] H. Tang, K.W. Schwarz, H.D. Espinosa, Phys. Rev. Lett. 100 (2008) 185503.
[28] Z. Yang, F. Jiao, Z. Lu, Z. Wang, Sci. China Phys. Mech. Astron. 56 (2013) 498–505.
[29] S. Plimpton, J. Comput. Phys. 117 (1995) 1–19.
[30] S.M. Foiles, M.I. Baskes, M.S. Daw, Phys. Rev. B 33 (1986) 7983–7991.
[31] J. Ziegler, J. Biersack, U. Littmark, The Stopping and Range of Ions in Solids, first ed., vol. 1, Pergamon Press, Oxford, 1985.
[32] A. Stukowski, Model. Simul. Mater. Sci. Eng. 18 (2010) 015012.
[33] A. Stukowski, Model. Simul. Mater. Sci. Eng. 20 (2012) 045021.
[34] G.J. Ackland, A.P. Jones, Phys. Rev. B 73 (2006) 054104.
[35] S. Davis, C. Loyola, F. González, J. Peralta, Comput. Phys. Commun. 181 (2010) 2126–2139.
[36] Y. Matsukawa, Y.N. Osetsky, R.E. Stoller, S.J. Zinkle, Philos. Mag. 88 (2008) 581–597.
[37] K. Nordlund, M. Ghaly, R.S. Averback, M. Caturla, T. Diaz de la Rubia, J. Tarus, Phys. Rev. B 57 (1998) 7556–7570.

[38] A.V. Krasheninnikov, K. Nordlund, J. Appl. Phys. 107 (2010) 071301.
[39] T.D. de la Rubia, R.S. Averback, R. Benedek, W.E. King, Phys. Rev. Lett. 59 (1987) 1930–1933.
[40] J. Wang, F. Sansoz, J. Huang, Y. Liu, S. Sun, Z.Z.S.X. Mao, Nat. Commun. 4 (2012) 1742.
[41] E.M. Bringa, K. Rosolankova, R.E. Rudd, B.A. Remington, J.S. Wark, M. Duchaine, D.H. Kalantar, J. Hawreliak, J.T. Belak, Nat. Mater. 5 (2006) 805–809.
[42] J. Rodriguez-Nieva, C. Ruestes, Y. Tang, E. Bringa, Acta Mater. 80 (2014) 67–76.